RSC Advances

PAPER

View Article Online
View Journal | View Issue

Cite this: *RSC Adv.*, 2022, **12**, 34815

Facile synthesis of phycocyanin/polydopamine hierarchical nanocomposites for synergizing PTT/PDT against cancer†

Huazhen Liang, ‡[a] Yaling Sun,‡[b] Chaoming Li,[a] Huaming Lin,[a] Qiwen Huang*[c] and Changguo Li *[a]

The exceptional biocompatibility and biosafety of natural proteins have made them a popular choice for tumor therapy in recent years, but their therapeutic effectiveness is severely constrained by factors including physiological instability, insufficient delivery, limited accumulation in tumor cells, *etc.* Here, a novel Mn-doped phycocyanin (Pc)/polydopamine (PDA) hierarchical nanostructure (MnPc@P) with excellent optical absorption, photothermal conversion, and photodynamic performances, is first designed and fabricated by a simply one-pot reaction, which not only successfully encapsulates natural protein Pc with intact activity in the nanostructure of MnPc@P but also gives them better biocompatibility. Upon laser irradiation, PDA-mediated hyperthermia and Pc-induced ROS elevation in tumor cells have been demonstrated, leading to drastic tumor cell death *via* combined PTT/PDT effect, greater than single PTT or PDT. In general, the expert fusion of Pc and PDA into a single nanomedicine opens fascinating perspectives in the delivery of natural proteins and tumor therapy.

Received 17th September 2022
Accepted 12th November 2022

DOI: 10.1039/d2ra05863d

rsc.li/rsc-advances

1. Introduction

Photodynamic therapy (PDT) is an emerging and promising noninvasive cancer treatment modality that employs exogenous light as the energy donor to specifically activate photosensitizer drugs (PSs) pre-localized in tumor cells and then converts surrounding O_2/H_2O into virulent reactive oxygen species (ROS, including $^1O_2/\cdot O_2^-$) to damage cellular content through energy transportation and translation.[1–6] As a key player in this photodynamic process, PSs determined the reaction rate, intensity, and ROS yield, all of which are strongly correlated with the species, biocompatibility, and accumulation of PSs in diseased tissue.[7–9] In recent years, researchers found that some natural proteins containing porphyrin structures, superior to representative organic porphyrin molecules, are capable of serving as desired PSs to improve tumor accumulation while reducing harmful effects to the body.[10–14] However, the biological application of protein-based PSs, which are now solely confined to hemoglobin and phycocyanin (Pc), is still in its infancy particularly in cancer therapy, which is severely hampered by physiologic instability and delivery difficulties.[15–18]

Along with the vigorous development of nanotechnology and nanomedicine, natural proteins have been extensively designed and utilized to participate in chemical reactions of nanomaterials' preparation as stabilizers or bio-components, which is also known as biomineralization.[19–22] Typically, bovine serum albumin (BSA) with abundant amino and carboxyl groups could coordinate with metal ions (such as Mn^{2+}) at first and therewith initiated biomineralization reaction in alkaline condition to form BSA-coated metal oxide nanoclusters such as manganese dioxide for cancer photo-theranostics.[23–27] Because of the BSA protection, the prepared manganese dioxide exhibited high biocompatibility and biosafety, which are essential requirements for upcoming clinical trials.[28–30] Therefore, the successful introduction and integration of natural proteins into the manufacture of nanomedicine is considered as a new era for cancer therapy, especially functionalized proteins like Pc.

Interestingly, another mussel-inspired polydopamine (PDA) that polymerized from biological dopamine monomer under alkaline conditions has been extensively applied in the biomedical field with good biocompatibility, easily modification, and tunable photophysical properties.[31–34] Their biological role in the field of cancer therapy, however, is incredibly single and solely involved photothermal therapy (PTT), which is unable to totally eradicate tumor cells.[35–38] Furthermore, to the best of our knowledge, it is yet illegal to intelligently combine functionalized proteins with PDA into a single nanomedicine through a simply one-pot procedure. Inspired by similar

[a]*Department of Oncology, Maoming People's Hospital, Maoming, 525000, Guangdong, China. E-mail: licgmm@163.com*

[b]*Department of Radiation Oncology, The Third Affiliated Hospital of Sun Yat-Sen University, Guangzhou, 510630, Guangdong, China*

[c]*Department of Pathology, Maoming People's Hospital, Maoming, 525000, Guangdong, China. E-mail: huangqiwen163163@163.com*

† Electronic supplementary information (ESI) available. See DOI: https://doi.org/10.1039/d2ra05863d

‡ These authors contributed equally to this work.

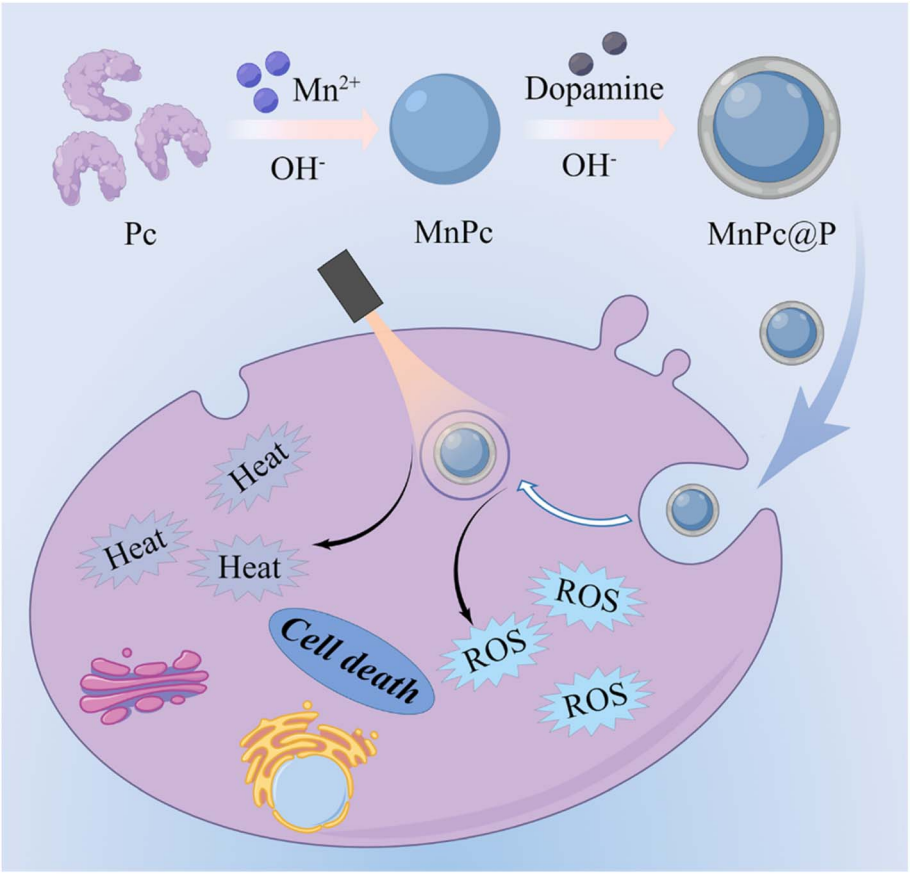

Fig. 1 Schematic illustration of the synthesis of MnPc@P NPs and the use of MnPc@P NPs for light-mediated PTT/PDT of tumors.

preparation processes of biomineralization and PDA, herein, we innovatively fabricated Mn-doped Pc/PDA hierarchical nanoparticles (MnPc@P NPs) under slightly alkaline conditions and successfully encapsulated natural protein Pc within nanostructure (Fig. 1). The prepared MnPc@P NPs exhibited good biocompatibility, excellent optical absorption, photothermal conversion, and photodynamic performances, resulting in locally hyperthermia and ROS production in tumor cells. Through combining PDA-mediated PTT and Pc-induced PDT, obvious tumor cell death could be achieved, more intense than either PTT or PDT alone. Overall, the successful marriage of PDA and MnPc into one nanomedicine will become a promising therapeutic strategy to achieve secure and effective tumor inhibition.

2. Experimental section

2.1 Materials

Dopamine hydrochloride and 1,3-diphenylisobenzofuran (DPBF) were obtained from Sigma-Aldrich. Manganese chloride ($MnCl_2$) and sodium hydroxide (NaOH) were purchased from Aladdin Biochemical Technology Co. (China). Phycocyanin (Pc) was purchased from Binmei Biotechnology Co., Ltd., China. Propidium iodide (PI), calcein-AM, cell counting kit-8 (CCK-8), and 2′,7′-dichlorofluorescin diacetate (DCFH-DA) were obtained from Beyotime (China). All above chemicals were used directly without further purification.

2.2 Synthesis of MnPc@P NPs

Firstly, 200 mg Pc was mixed with 20 mL of deionized water (Di H_2O) and then gently stirred for several minutes. Afterward, the freshly prepared $MnCl_2$ aqueous solution (1 mL, 12.6 mg mL^{-1}) and 36 mg dopamine hydrochloride were slowly added into the above mixture and stirred for 2.5 h to obtain complex. Subsequently, the pH of complex solution was adjusted to about 10 by using 1 M NaOH or HCl and stirred for another 4 h at room temperature. The resulting MnPc@P NPs were collected by centrifugating and washing with Di H_2O repeatedly, and finally dispersed in deionized water for future use.

2.3 Characterization

Transmission electron microscopy (TEM) images were acquired on a JEM-2100UHR microscope (JEOL, Japan) to characterize the morphology. X-ray photoelectron spectroscopy (XPS, ESCALAB 250Xi, Japan) was applied to analyze the chemical compositions of MnPc@P. UV-vis-NIR spectrum was investigated by using an Infinite M200 PRO spectrophotometer. The hydrodynamic particle size and zeta potential of MnPc@P was monitored by dynamic light scattering (DLS, 15 mW laser, 676 nm incident beam; Brookhaven Instruments Corporation).

2.4 Photothermal conversion performance of MnPc@P NPs

To systematically evaluate the photothermal conversion performance of MnPc@P NPs, the increase in temperature of MnPc@P NPs was monitored by exposing MnPc@P aqueous solutions with different concentrations (0, 50, 100, 200, and 400 μg mL^{-1}) to 808 nm laser at different power densities (0.5, 1.0, 1.5 and 2.0 W cm^{-2}) for 5 min using an IR thermal camera (TI100 Infrared Camera FLK-TI100 9HZ, FLUKE). Deionized water was irradiated as a control. To study the photothermal stability, MnPc@P aqueous solution (200 μg mL^{-1}) was irradiated by an 808 nm laser at the same power density of 1.0 W cm^{-2} for five repeated cycles of 6 min irradiation ON and 9 min OFF.

2.5 Photodynamic performance of MnPc@P NPs

1,3-Diphenylisobenzofuran (DPBF) probe is widely used to detect the generation of $^1O_2$. Briefly, 200 μg mL^{-1} of MnPc@P aqueous solution was taken with 20 μL of DPBF (1.5 mg mL^{-1}, pre-dissolved in ethanol). Then, this mixed solution was exposed to a 660 nm laser at 400 mW cm^{-2} power density for different time (0, 4, 8, 12, 16, 20, 24, and 28 min) and instantly measured by using a UV-vis-NIR spectrometer.

2.6 Cell culture

Human breast cancer cells (MCF-7, obtained from American Type Culture Collection) were cultured and maintained in Dulbecco's Modified Eagle's Medium (DMEM) consisting 10% FBS supplemented with 100 U per mL penicillin and 100 μg per mL streptomycin. The cultures were maintained at 37 °C in a humidified atmosphere with 5% CO_2.

2.7 Cytotoxicity of MnPc@P NPs

MCF-7 cells were seeded in 96 well plates at the density of 8×10^3 cells per well and cultured overnight. Then, different concentrations (0, 3.13, 6.25, 12.5, 25, 50, 100, and 200 μg mL^{-1}) of MnPc@P NPs were added to replace the medium. After incubated for 24 or 48 h, the cell viability assay was conducted following the standard protocol to detect the relative cell viability by using the SpectraMax M2 plate reader (Molecular Devices, CA, USA).

To evaluate *in vitro* photo-toxicity of MnPc@P NPs, MCF-7 cancer cells (8×10^3 cells per well) were co-cultured with MnPc@P NPs with various concentrations (0, 3.13, 6.25, 12.5, 25, 50, 100, and 200 μg mL^{-1}) for 6 h. Afterwards, the cells were irradiated with 660 nm (400 mW cm^{-2}) or 808 nm laser (1.0 W cm^{-2}) for 5 min and incubated for another 24 h. Finally, cell viabilities were determined by CCK-8 assay. The calcein-AM (4×10^{-6} M) and PI solution (4×10^{-6} M) were employed to evaluate the live and dead cells by confocal laser scanning microscope (CLSM, Zeiss-800, Germany).

2.8 Intracellular ROS detection

MCF-7 cells were seeded in the confocal dish with a density of 2×10^5 cells to adhere and then co-cultured with pure DMEM or MnPc@P (200 μg mL^{-1}) for 6 h. The cells in laser treatment groups were exposed to a 660 nm laser (400 mW cm^{-2}) for 5 min. For intracellular ROS generation, the cells were stained with DCFH-DA (20 μM) for 30 min. Thereafter, the intracellular ROS were qualitatively determined using CLSM.

3. Results and discussion

3.1 Preparation and characterization of MnPc@P NPs

The MnPc@P NPs was simply synthesized by a one-pot reaction, in which Pc as biomineralizing molecules to bond with Mn^{2+} and whereafter conducted biomimetic mineralization procedure under an alkaline condition, in conjunction with the polymerization of dopamine hydrochloride. As illustrated in Fig. 2a, the prepared MnPc@P NPs exhibited an irregular spherical morphology with a particle size of approximately 60 nm. In contrast, because of the aggregation effect and hydration layer, the hydrodynamic diameter of NPs was increased to about 170 nm and the homologous zeta potential was −20.11 mV, which were favorable for blood circulation (Fig. 2b, c and S1†). The reason for their negative charge was attributed to the doped Pc proteins and the rich phenolic hydroxyl groups in PDA.[39] In addition, the good dispersibility of NPs was shown in the digital image of MnPc@P NPs distributed in several physiological mediums (pure water, PBS, and DMEM), with no obvious sedimentation or agglomeration (Fig. 2d). As shown in Fig. S2,† MnPc@P NPs maintained good colloidal stability in PBS for a period of 48 h, with just a 27 nm size increase over that at 0 h. After that, the chemical composition of MnPc@P NPs was also the focus of the issue and investigated through X-ray photoelectron spectroscopy (XPS). From the survey spectrum in Fig. 2e, the elements of C, N, O, and Mn were all detected in MnPc@P nanostructure. To further understand the metal valence state of Mn element, the high-resolution XPS spectra of Mn 2p was thoroughly analyzed. The peaks at 641.0 and 653.1 eV were assigned to Mn $2p_{3/2}$ and Mn $2p_{1/2}$, respectively, manifesting tetravalent state of Mn element in MnPc@P NPs (Fig. 2f).

3.2 Photothermal and photodynamic performances of MnPc@P NPs

Strong optical absorption and light conversion efficiency are essential for photo-responsive agents (whether photosensitizers or photothermal agents), as they guarantee significant ROS output or pronounced temperature elevation. Initially, the ultraviolet-visible spectrophotometer was applied to analyze the optical absorption performance of MnPc@P NPs. As displayed in Fig. 3a, MnPc@P NPs presented broad optical absorbance between 400 nm to 900 nm, which steadily rose with concentration enhancement, particularly at 660 nm and 808 nm laser wavelengths (Fig. S3†). Subsequently, the photothermal conversion efficiency of MnPc@P aqueous solution was assessed by keeping track of the temperature change in real-time while being exposed to an 808 nm laser beam. As expected, MnPc@P exhibited concentration- and power-dependent temperature increases (Fig. 3b and c). After receiving 808 nm laser irradiation (1.0 W cm^{-2}) for 5 min, the temperature change (ΔT) of MnPc@P at concentration of 200

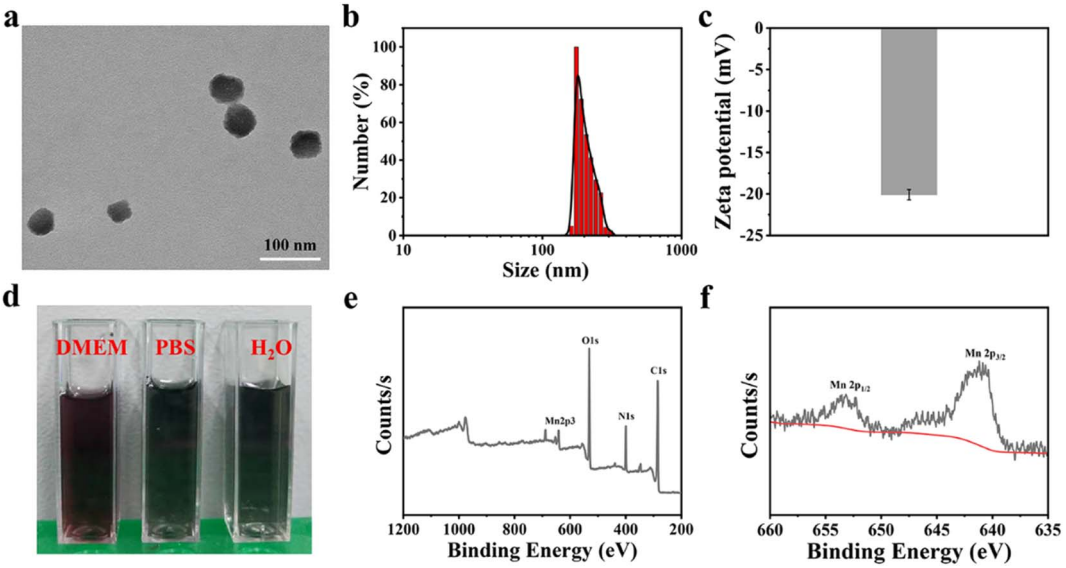

Fig. 2 (a) TEM image, (b) size distribution, and (c) zeta potentials of MnPc@P NPs. (d) The digital images of MnPc@P NPs dispersed in pure water, PBS, and DMEM. (e) XPS spectrum of MnPc@P NPs and (f) the corresponding high-resolution Mn 2p XPS spectrum.

and 400 μg mL^{-1} could increase by 28.0 and 40.7 °C, respectively. In contrast, a negligible temperature increase was observed in pure water exposed to the same irradiation, demonstrating that MnPc@P could efficiently and quickly convert 808 nm photon energy into thermal energy. Furthermore, the photostability was also an important parameter to reflect their optical property. Under five laser on/off cycles, the similar temperature increment of MnPc@P was observed in each cycle, indicating the good photothermal conversion stability (Fig. 3d and S4†). Furthermore, the photothermal conversion efficiency (η) of MnPc@P NPs was calculated to be 14.27%.

As previously mentioned, Pc can act as photosensitizers to transform surrounding O_2 into toxicity $^1O_2$ when exposed to laser. Therefore, the $^1O_2$ generated ability of MnPc@P NPs was investigated by using 1,3-diphenylisobenzofuran (DPBF) as a detection reagent. Under 660 nm laser exposure, the DPBF degradation percentage of MnPc@P treated group gradually

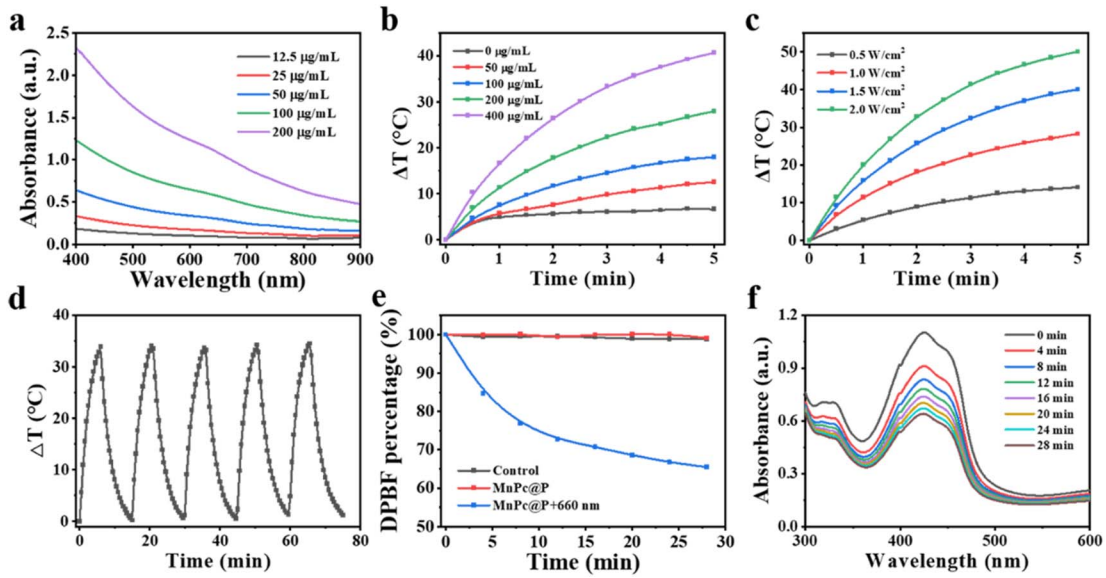

Fig. 3 (a) UV-vis-NIR spectra of various concentrations of MnPc@P NPs. (b) Temperature change profiles of MnPc@P NPs with different concentrations under 808 nm laser irradiation for 5 min at the power density of 1.0 W cm^{-2}. (c) Temperature change profiles of MnPc@P NPs exposed to different power densities (0.5–2.0 W cm^{-2}) of 808 nm laser. (d) Photothermal conversion stability of MnPc@P NPs aqueous solution for five laser on/off cycles under the irradiation of 808 nm laser. (e) The degradation of DPBF caused by different treatments including control, MnPc@P, and MnPc@P + 660 nm. (f) The degradation of DPBF caused by MnPc@P + 660 nm treatment group.

increased with time extension (Fig. 3e and f). In sharp contrast, the single MnPc@P treated group without laser exposure produced negligible $^1O_2$ during the measured time. According to those findings, MnPc@P functioning as photosensitizers has the capacity to produce abundant ROS to destroy tumor cells when exposed to laser irradiation.

3.3 Cytotoxicity and ROS generation

Encouraged by the above excellent photothermal conversion and photodynamic performances of MnPc@P NPs, we further assessed their combined antitumor efficiency at the cellular level. Without the stimulation of exogenous laser, only MnPc@P-treated MCF-7 cells maintained relatively high cell viability (above 85%) after 24 or 48 h of incubation, even at the maximum concentration of 200 μg mL^{-1} (Fig. 4a). The results demonstrated good biocompatibility of MnPc@P NPs. However, in sharp contrast, when MnPc@P-treated cells were subjected to a 660 nm laser for 5 min, concentration-dependent cell death was achieved and reached as high as 40% and 68% at the concentrations of 100 and 200 μg mL^{-1}, respectively (Fig. 4b). The reason for the remarkable cytotoxicity was attributed to the photodynamic property of MnPc@P NPs activated by 660 nm laser, which caused the ROS generation in tumor cells as shown and proved by the emerge green fluorescence of DCF produced by the reaction of ROS and DCFH-DA probes (Fig. 5). Analogously, through switching the energy source from a 660 nm

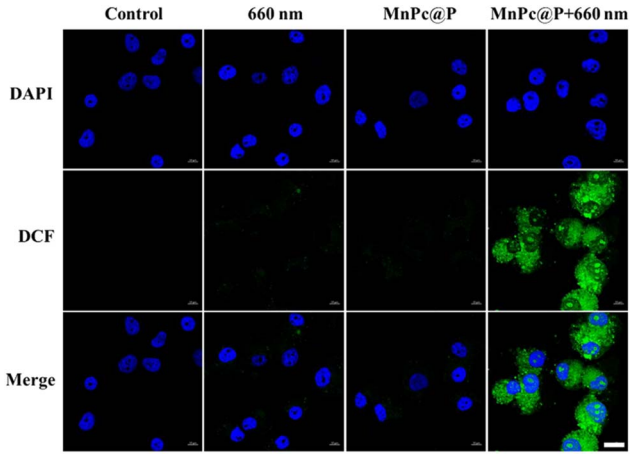

Fig. 5 CLSM images of intracellular ROS in MCF-7 cells after different treatments, scale bar: 20 μm.

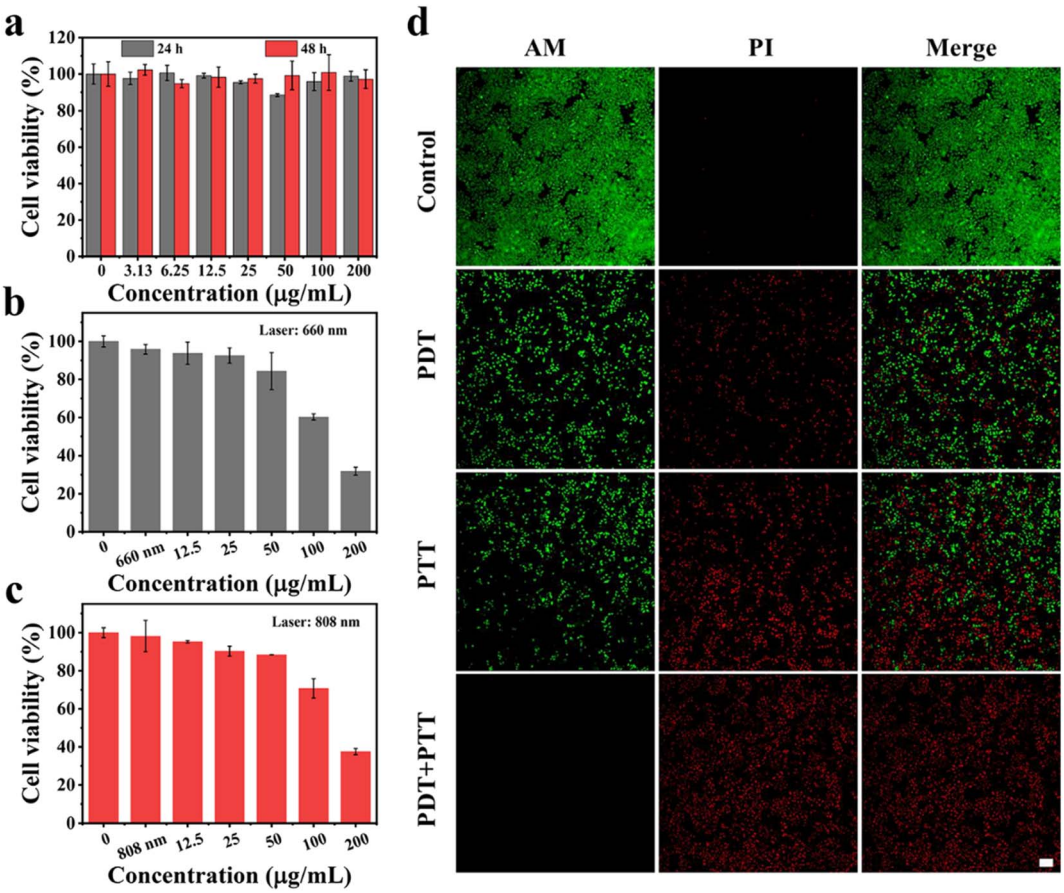

Fig. 4 (a) Relative viabilities of MCF-7 cells treated with different concentrations of MnPc@P NPs (0, 3.13, 6.25, 12.5, 25, 50, 100, and 200 μg mL^{-1}) for 24 or 48 h. Relative viabilities of MCF-7 cells after being treated with MnPc@P NPs under (b) a 660 nm laser irradiation (0.4 W cm^{-2}) or (c) an 808 nm laser irradiation (1.0 W cm^{-2}) for 5 min. (d) Fluorescence images of MCF-7 cells stained by calcein-AM (green) and PI (red) after different treatment, scale bar: 200 μm.

laser to an 808 nm laser, the photothermal conversion performance of MnPc@P could be activated to cause a local temperature rise and damage tumor cells. As seen in Fig. 4c, the viability of MCF-7 cells constantly declined as MnPc@P concentrations rose. More importantly, compared to either a single PTT effect or a single PDT effect, MnPc@P exhibited higher cell toxicity to MCF-7 cells after exerting PTT and PDT effect together (Fig. 4d). Overall, those results suggested that by combining PDT and PTT effect, the developed MnPc@P NPs has the potential to be an outstanding photosensitizer and photothermal agent for the elimination of tumor cells.

4. Conclusions

In conclusion, for the first time, the skillfully integration of natural protein Pc and PDA into one nanomedicine (MnPc@P) was successfully constructed under alkaline conditions by a straightforward one-pot reaction using Mn^{2+} as coupling agents. Due to the intact encapsulation of Pc and the polymerization of dopamine, MnPc@P NPs displayed good biocompatibility, excellent photothermal conversion, and photodynamic performances, which endowed them with the abilities to produce locally hyperthermia and abundant $^1O_2$ under the laser irradiation of different wavelengths (660 or 808 nm), thus inducing serious damage to tumor cells. More importantly, even after 48 h of co-incubation, MnPc@P showed insignificant toxicity to cells in the absence of irradiation. This work promoted the development of phototherapy technique based on a natural protein Pc that exhibits exceptional photodynamic performance and expands biomineralization preparation.

Conflicts of interest

There are no conflicts to declare.

Acknowledgements

This work was financially supported by the Maoming Science and Technology Plan (No. 2021555) and the High-level Hospital Construction Research Project of Maoming People's Hospital (No. zx2020020).

Notes and references

1 P. C. Lo, M. S. Rodriguez-Morgade, R. K. Pandey, D. K. P. Ng, T. Torres and F. Dumoulin, *Chem. Soc. Rev.*, 2020, **49**, 1041–1056.
2 P. T. Chung, N. Van-Nghia, Y. Choi, S. Lee and J. Yoon, *Chem. Rev.*, 2021, **121**, 13454–13619.
3 H. Chen, T. Sun, W. Zeng, X. Zeng, L. Mei, C. Jiang and Y. Zhao, *ACS Mater. Lett.*, 2022, **4**, 111–119.
4 M. Zhang, X. Qin, W. Xu, Y. Wang, Y. Song, S. Garg and Y. Luan, *J. Colloid Interface Sci.*, 2021, **594**, 493–501.
5 J. Zhang, N. Wang, Q. Li, Y. Zhou and Y. Luan, *Chem. Commun.*, 2021, **57**, 2305.
6 Y. Yi, M. Yu, C. Feng, H. Hao, W. Zeng, C. Lin, H. Chen, F. Lv, D. Zhu, X. Ji, L. Mei, M. Wu and W. Tao, *Matter*, 2022, **5**, 2285–2305.
7 X. Li, J. F. Lovell, J. Yoon and X. Chen, *Nat. Rev. Clin. Oncol.*, 2020, **17**, 657–674.
8 J. Xie, Y. Wang, W. Choi, P. Jangili, Y. Ge, Y. Xu, J. Kang, L. Liu, B. Zhang, Z. Xie, J. He, N. Xie, G. Nie, H. Zhang and J. S. Kim, *Chem. Soc. Rev.*, 2021, **50**, 9152–9201.
9 W. Zeng, H. Zhang, X. Yuan, T. Chen, Z. Pei and X. Ji, *Adv. Drug Delivery Rev.*, 2022, **184**, 114241.
10 L. Jiang, H. Bai, L. Liu, F. Lv, X. Ren and S. Wang, *Angew. Chem., Int. Ed.*, 2019, **58**, 10660–10665.
11 W. Li, J. Yang, L. Luo, M. Jiang, B. Qin, H. Yin, C. Zhu, X. Yuan, J. Zhang, Z. Luo, Y. Du, Q. Li, Y. Lou, Y. Qiu and I. You, *Nat. Commun.*, 2019, **10**, 3349.
12 D. Chen, M. Suo, J. Guo, W. Tang, W. Jiang, Y. Liu and Y. Duo, *Adv. Healthcare Mater.*, 2021, **10**, 2001577.
13 D. H. Wan, B. Y. Zheng, M. R. Ke, J. Y. Duan, Y. Q. Zheng, C. K. Yeh and J. D. Huang, *Chem. Commun.*, 2017, **53**, 4112–4115.
14 W. Zhang, L. Yu, Y. Jiang and C. Guo, *Biomater. Sci.*, 2021, **9**, 5302–5318.
15 Y. Yang, W. Zeng, P. Huang, X. Zeng and L. Mei, *View*, 2021, **2**, 20200042.
16 M. Delfi, R. Sartorius, M. Ashrafizadeh, E. Sharifi, Y. Zhang, P. De Berardinis, A. Zarrabi, R. S. Varma, F. R. Tay, B. R. Smith and P. Makvandi, *Nano Today*, 2021, **38**, 101119.
17 O. S. Fenton, K. N. Olafson, P. S. Pillai, M. J. Mitchell and R. Langer, *Adv. Mater.*, 2018, **30**, 1705328.
18 H. Nakamura, F. Jun and H. Maeda, *Expert Opin. Drug Delivery*, 2015, **12**, 53–64.
19 K. Liang, R. Ricco, C. M. Doherty, M. J. Styles, S. Bell, N. Kirby, S. Mudie, D. Haylock, A. J. Hill, C. J. Doonan and P. Falcaro, *Nat. Commun.*, 2015, **6**, 7240.
20 V. S. Tagliabracci, J. L. Engel, J. Wen, S. E. Wiley, C. A. Worby, L. N. Kinch, J. Xiao, N. V. Grishin and J. E. Dixon, *Science*, 2012, **336**, 1150–1153.
21 R. Xing, K. Liu, T. Jiao, N. Zhang, K. Ma, R. Zhang, Q. Zou, G. Ma and X. Yan, *Adv. Mater.*, 2016, **28**, 3669–3676.
22 B. Yang, J. Yin, Y. Chen, S. Pan, H. Yao, Y. Gao and J. Shi, *Adv. Mater.*, 2018, **30**, 1705611.
23 P. Prasad, C. R. Gordijo, A. Z. Abbasi, A. Maeda, A. Ip, A. M. Rauth, R. S. DaCosta and X. Y. Wu, *ACS Nano*, 2014, **8**, 3202–3212.
24 W. Tang, W. Fan, W. Zhang, Z. Yang, L. Li, Z. Wang, Y. L. Chiang, Y. Liu, L. Deng, L. He, Z. Shen, O. Jacobson, M. A. Aronova, A. Jin, J. Xie and X. Chen, *Adv. Mater.*, 2019, **31**, 1900401.
25 X. Liu, Q. Wang, H. Zhao, L. Zhang, Y. Su and Y. Lv, *Analyst*, 2012, **137**, 4552–4558.
26 J. Pan, Y. Wang, H. Pan, C. Zhang, X. Zhang, Y. Y. Fu, X. Zhang, C. Yu, S. K. Sun and X. P. Yan, *Adv. Funct. Mater.*, 2017, **27**, 1603440.
27 Y. Wang, Y. Song, G. Zhu, D. Zhang and X. Liu, *Chin. Chem. Lett.*, 2018, **29**, 1685–1688.
28 S. F. Kiew, L. V. Kiew, H. B. Lee, T. Imae and L. Y. Chung, *J. Controlled Release*, 2016, **226**, 217–228.

29 Y. Jin, H. Wang, K. Yi, S. Lv, H. Hu, M. Li and Y. Tao, *Nano-Micro Lett.*, 2021, **13**, 25.
30 A. O. Elzoghby, W. M. Samy and N. A. Elgindy, *J. Controlled Release*, 2012, **157**, 168–182.
31 W. Cheng, X. Zeng, H. Chen, Z. Li, W. Zeng, L. Mei and Y. Zhao, *ACS Nano*, 2019, **13**, 8537–8565.
32 J. Qin, L. Guo, T. Yang, X. Wu, Z. Wang, F. Xie and H. Peng, *ChemNanoMat*, 2021, **7**, 1322–1329.
33 L. Guo, Q. Xia, J. Qin, M. Yang, T. Yang, F. You, Z. Chen, B. Liu and H. Peng, *J. Colloid Interface Sci.*, 2021, **616**, 81–92.
34 W. Zeng, H. Zhang, Y. Deng, A. Jiang, X. Bao, M. Guo, Z. Li, M. Wu, X. Ji, X. Zeng and L. Mei, *Chem. Eng. J.*, 2020, **389**, 124494.
35 F. Ding, X. Gao, X. Huang, H. Ge, M. Xie, J. Qian, J. Song, Y. Li, X. Zhu and C. Zhang, *Biomaterials*, 2020, **245**, 119976.
36 L. S. Lin, Z. X. Cong, J. B. Cao, K. M. Ke, Q. L. Peng, J. Gao, H. H. Yang, G. Liu and X. Chen, *ACS Nano*, 2014, **8**, 3876–3883.
37 X. Wang, J. Zhang, Y. Wang, C. Wang, J. Xiao, Q. Zhang and Y. Cheng, *Biomaterials*, 2016, **81**, 114–124.
38 P. Yang, F. Zhu, Z. Zhang, Y. Cheng, Z. Wang and Y. Li, *Chem. Soc. Rev.*, 2021, **50**, 8319–8343.
39 Q. Deng, P. Sun, L. Zhang, Z. Liu, H. Wang, J. Ren and X. Qu, *Adv. Funct. Mater.*, 2019, **29**, 1903018.